Full Dimensional Quantum Calculations of Vibrational Energies of $H_5O_2^+$†

Xinchuan Huang,‡ Hyung Min Cho,§ Stuart Carter,‡,⊥ Lars Ojamäe,|| Joel M. Bowman,*,‡ and Sherwin J. Singer§,#

Cherry L. Emerson Center of Scientific Computation and Department of Chemistry, Emory University, Atlanta, Georgia 30322, Department of Chemistry, The Ohio State University, 100 W. 18th Avenue, Columbus, Ohio 43210, and Department of Chemistry, IFM, Linköping University, SE-581 83 Linköping, Sweden

Received: April 22, 2003; In Final Form: July 3, 2003

Two full dimensional (15 degrees-of-freedom) quantum calculations of vibrational energies of $H_5O_2^+$ are reported using the global potential energy surface (OSS) of Ojamäe et al. (*J. Chem. Phys.* **1998**, *109*, 5547). One set of calculations uses the diffusion Monte Carlo (DMC) method with a highly flexible initial trial wave function. This method is limited to the ground vibrational state, but produces what we believe is a highly accurate, benchmark energy and wave function for that state. The DMC wave function is analyzed to identify coordinates that are strongly correlated in zero-point fluctuations. A simple harmonic model is developed to elucidate the energetic consequences of these correlations. The other set of calculations is based on the code MULTIMODE, which does configuration interaction (CI) calculations using a basis determined from a vibrational self-consistent field (VSCF) Hamiltonian, but which uses a representation of the potential with mode coupling limited to a maximum of four modes. Good agreement is obtained between the DMC and the CI MULTIMODE energies for the ground vibrational state. When less sophisticated theoretical treatments are applied, either variational Monte Carlo or vibrational self-consistent field, fairly large errors are found. Vibrationally excited-state energies obtained with MULTIMODE are also reported.

I. Introduction

The protonated water dimer, $H_5O_2^+$, also known as the Zundel cation, has been the subject of extensive experimental and theoretical studies for over 30 years. This was motivated by its important role in proton solvation and transfer processes in aqueous solutions. For the ion formation reaction

$$H_3O^+ + H_2O \leftrightarrow H_5O_2^+$$

experimental thermodynamics studies[1−5] have reached excellent agreement with theoretical predictions[6−13] on binding energies, ≈33 kcal/mol. The temperature dependence of the equilibrium constant and rate constant have also been estimated in kinetics studies.[2,4]

In the 1960s, X-ray diffraction expriments[14] determined $H_5O_2^+$ as a C_2 structure in the hydrate crystal. Later, high-level ab initio calculations[6,10,12,15−25] mainly confirmed that $H_5O_2^+$ has a C_2 minimum geometry in its electronic ground state: two strong H-bonds connect the two terminal $-H_2O$ equally, with its O···H$^+$···O backbone being slightly nonlinear ($\angle$OHO ≈ 174°, R_e ≈ 1.20 Å).[16] This differs from its isoelectronic ion, $N_2H_7^+$, which is predicted[26−29] to be more stable with an asymmetric NH_4^+ ···NH_3 configuration. The earliest geometry optimizations with modest basis sets found $H_5O_2^+$ to have a staggered D_{2d} minimum,[13,30,31] or C_s minimum in which the proton is bonded more closely to one oxygen atom than to the other; i.e., there is one covalent bond and one H-bond. Even in high-level ab initio geometry optimizations, the C_s transition state ($\angle$OHO ≈ 176°, R_{e1} ≈ 1.13 Å, R_{e2} ≈ 1.26 Å)[16] is only approximately 0.4 kcal/mol higher than the C_2 minimum.[6,10,16] This suggests that, under C_2 symmetry, the competition between covalent contributions and electrostatic ion−dipole forces results in rather a flat minimum on the potential energy surface.[6,10,25,32−34]

A large number of $H_5O_2^+$ spectral studies[35−42] have been done in various condensed environments, such as zeolites, salts and acid solutions. Because of the highly delocalized charge[13,30,31,43] and extra high polarizability,[25,44] the $H_5O_2^+$ ion has a continuous[40−42] and intense[35] absorption spectrum between 1000 and 3400 cm^{-1}. The gas-phase vibrational spectrum of $H_5O_2^+$ is still far from complete. In 1989, Yeh and Okumura et al.[45,46] reported band origins for the symmetric and asymmetric OH− stretch modes at 3608.8 and 3684.4 cm^{-1}, respectively.

Numerous theoretical studies have been devoted to the calculation of ab initio harmonic, normal-mode frequencies.[6,9,12,17,19,24,30,32,33,47] However, as pointed out in these studies, especially the recent ones of Valeev and Schaefer,[16] the flat minimum and strongly anharmonic proton-transfer motion make these harmonic predictions of limited value.

There have been a number of attempts to investigate the vibrational motion of $H_5O_2^+$ beyond the harmonic approximation. Most of these have been molecular dynamics calculations.[48−51] Two sets of approximate quantum calculations have been reported previously. One was in reduced dimensionality (3 and 4 degrees of freedom) by Vener et al.[32,33] and the other was a vibrational self-consistent field calculation, with perturbation theory corrections by Chaban et al.[52] This calculation used a

* Corresponding author. E-mail: bowman@euch4e.chem.emory.edu.
† Part of the special issue "Donald J. Kouri Festschrift".
‡ Emory University.
§ The Ohio State University.
⊥ Permanent address: Department of Chemistry, University of Reading, Reading, U.K.
|| Linköping University.
E-mail: singer@chemistry.ohio-state.edu.

10.1021/jp035081a CCC: $25.00
Published on Web 08/05/2003

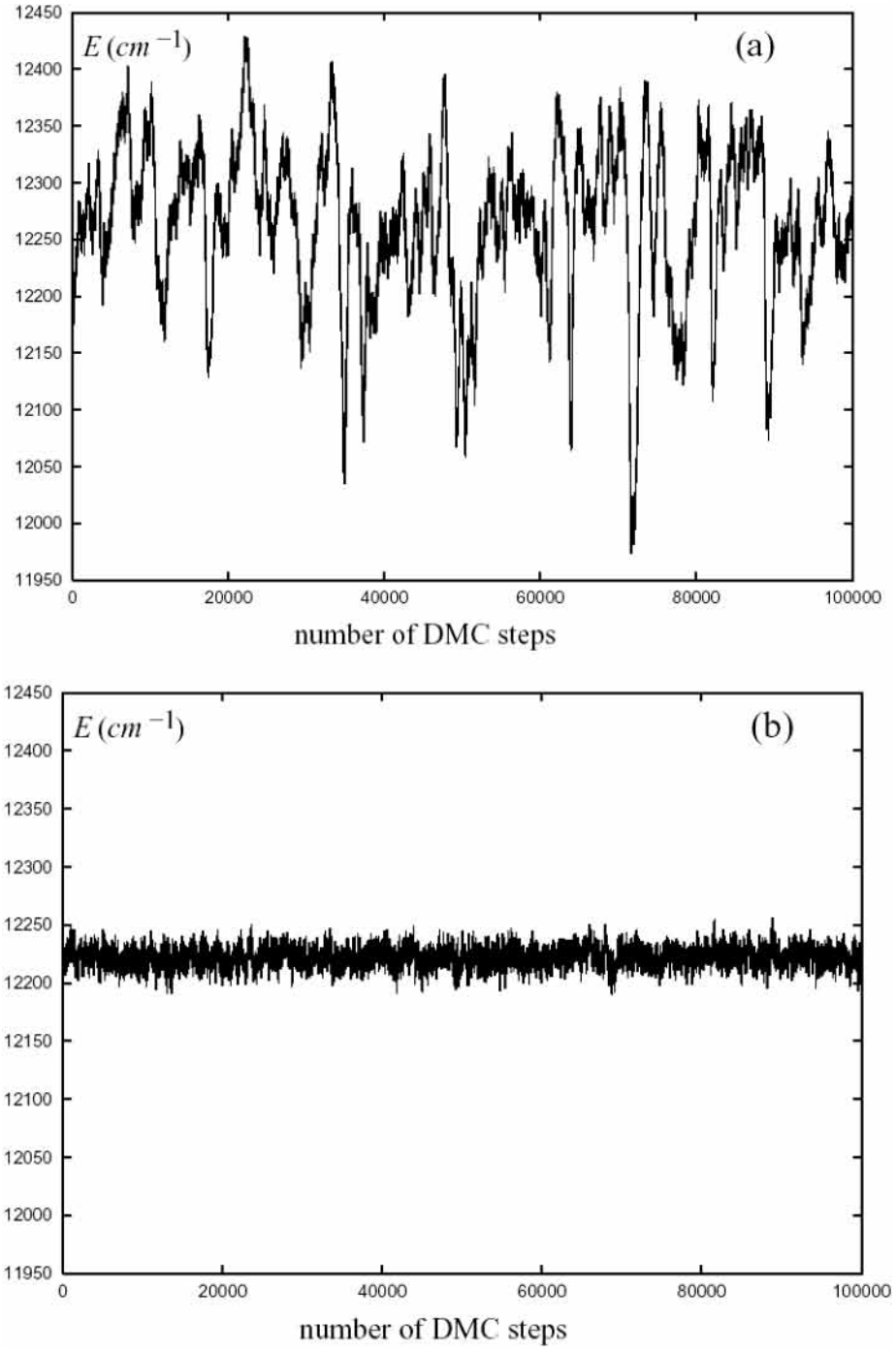

Figure 1. Local energy averaged $H\psi_{trial}/\psi_{trial}$ over 40000 walkers during a DMC calculation. Branching caused the number of walkers to fluctuate. The total remained close to 40 000 during the run. The trial wave function used in the calculation of panel a was not as high-quality as that of panel b, which, as depicted here, results in greater statistical errors in the estimation of the ground-state energy. (The trial wave function used to generate the data of panel a lacked the υ_9 and υ_{10} functions of eq 2 and also lacked the bottom three coupling terms in Table 2. Furthermore, υ_3 was taken to be a function of z, not z^2 as in eq 2.)

two-mode representation of the potential, the accuracy of which was not tested. Both calculations reported significant red-shifted deviations from corresponding harmonic normal mode energies.

An accurate, full-dimensional treatment of the vibrations of $H_5O_2^+$ is quite challenging, even beyond the challenge of the high dimensionality, owing to a large degree of "floppiness". A careful analysis of several possible internal low-energy rearrangements has been reported recently by Wales.[15] The calculated barrier heights of these internal motions are low enough (<1 kcal/mol) to possibly produce observable splittings in the spectrum. (The existence of such low-energy pathways was pointed out nearly 10 years ago; however, a search for possible splittings in a high-resolution spectrum was inconclusive.[53])

In this paper we report two efforts to obtain vibrational energies of $H_5O_2^+$ in full dimensionality. The first method we apply is the diffusion quantum Monte Carlo (DMC) method.[54−56] This method is applied only to the ground vibrational state, where in principle, it can provide the exact energy (the zero-point energy) and wave function. The second method is a vibrational configuration interaction method using a basis obtained from a vibrational self-consistent field (VSCF)

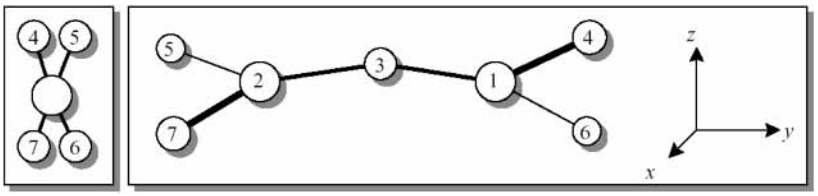

Figure 2. Schematic depiction of $H_5O_2^+$ in its equilibrium geometry, indicating the labeling of the atoms used in Table 1.

TABLE 1: Coordinates Used for $H_5O_2^+$ Guiding Function.

coordinate	definition	characterization
d_a	$\lvert\mathbf{r}_2 - \mathbf{r}_3\rvert$	inner proton to oxygen stretch
d_b	$\lvert\mathbf{r}_1 - \mathbf{r}_3\rvert$	inner proton to oxygen stretch
R	$\lvert\mathbf{r}_1 - \mathbf{r}_2\rvert$	oxygen−oxygen distance
z	$\lvert\mathbf{r}_3 - \mathbf{r}_A\rvert$	deviation of inner proton from oxygen−oxygen axis
d_{OH_1}	$\lvert\mathbf{r}_1 - \mathbf{r}_4\rvert$	outer oxygen−hydrogen stretch
d_{OH_2}	$\lvert\mathbf{r}_1 - \mathbf{r}_6\rvert$	outer oxygen−hydrogen stretch
d_{OH_3}	$\lvert\mathbf{r}_2 - \mathbf{r}_5\rvert$	outer oxygen−hydrogen stretch
d_{OH_4}	$\lvert\mathbf{r}_2 - \mathbf{r}_7\rvert$	outer oxygen−hydrogen stretch
d_{HH_a}	$\lvert\mathbf{r}_4 - \mathbf{r}_6\rvert$	outer hydrogen−hydrogen distance, a water bend coordinate
d_{HH_b}	$\lvert\mathbf{r}_5 - \mathbf{r}_7\rvert$	outer hydrogen−hydrogen distance, a water bend coordinate
ω_a	$(\mathbf{r}_B - \mathbf{r}_1)\cdot(\mathbf{r}_1 - \mathbf{r}_2)$	water molecule wag
ω_b	$(\mathbf{r}_C - \mathbf{r}_2)\cdot(\mathbf{r}_2 - \mathbf{r}_1)$	water molecule wag
Θ_{ab}	$[\{(\mathbf{r}_4 - \mathbf{r}_6)\cdot(\mathbf{r}_5 - \mathbf{r}_7)\}/\{\lvert\mathbf{r}_4 - \mathbf{r}_6\rvert\lvert\mathbf{r}_5 - \mathbf{r}_7\rvert\}]^2$	torsional coordinate measuring alignment of outer waters
Θ_a	$[\{(\mathbf{r}_4 - \mathbf{r}_6)\cdot(\mathbf{r}_3 - \mathbf{r}_A)\}/\{\lvert\mathbf{r}_4 - \mathbf{r}_6\rvert\}]^2$	torsional coordinate measuring alignment of waters with the direction by which the central proton deviates from the oxygen−oxygen bond
Θ_b	$[\{(\mathbf{r}_5 - \mathbf{r}_7)\cdot(\mathbf{r}_3 - \mathbf{r}_A)\}/\{\lvert\mathbf{r}_5 - \mathbf{r}_7\rvert\}]^2$	torsional coordinate measuring alignment of waters with the direction by which the central proton deviates from the oxygen−oxygen bond

[a]The definitions make use of several intermediate points: the midpoint of the oxygen−oxygen bond, $\mathbf{r}_A \equiv (1/2)(\mathbf{r}_1 + \mathbf{r}_2)$ and the two midpoints between outer hydrogen pairs, $\mathbf{r}_B \equiv (1/2)(\mathbf{r}_4 + \mathbf{r}_6)$ and $\mathbf{r}_C \equiv (1/2)(\mathbf{r}_5 + \mathbf{r}_7)$.

calculation.[57−59] For this calculation we use MULTIMODE, version 4.6,[59−63] denoted MM4.6. This is a general code that can be used to obtain vibrational energies of the ground and excited states of polyatomic molecules. The results from this code are not exact, due to an approximate treatment of the potential. Thus, a comparison with the highly accurate DMC results for the zero-point energy provides a rigorous test of the accuracy of MM4.6, at least for the ground vibrational state.

The potential energy surface we use belongs to the OSS1-3 family of potentials.[6,64] One of the version 3 surfaces, denoted as OSS3(p), was chosen. These surfaces were first reported in Ojamäe et al.[6] in 1995, and they have been well developed for simulations of water clusters with excess protons, $H^+(H_2O)_n$.[64,65] To calculate vibrational spectra and to simulate proton-transfer reactions, the OSS analytical potential energy models were constructed in such a way that they can describe both the intramolecular interactions and the intermolecular interactions, such as the interactions between H_3O^+ and H_2O in $H_5O_2^+$. These surfaces were assembled from a large number of MP2[66] calculations using Gaussian92,[67] utilizing the cc-pVTZ[68] basis set with diffuse basis functions on oxygen (aug-cc-pVTZ).[69] An analytical expression was fit by a nonlinear least-squares minimization to these ab initio energies. The potential functional form contains two-body interactions, three-body interactions, and electrostatic contributions.[64] It is one of the most extensive, full-dimensional surfaces available for protonated cluster ions.

This paper is organized as follows: Section II describes the DMC calculation details, analysis and results. The theoretical background and variational scheme implemented in MM4.6 is simply introduced in section III, along with results and comparison with the DMC calculations. A summary and discussion of the results are given in section IV.

II. Diffusion Monte Carlo Calculation

Computational Details. The efficiency of diffusion Monte Carlo (DMC) calculations is usually enhanced by importance sampling based on a trial wave function, or guiding function.[70−72] In principle, DMC will provide the true ground state energy for any choice of guiding function. In practice, especially for a large and floppy system such as $H_5O_2^+$, a good quality guiding function is needed to obtain highly accurate ground vibrational properties. Figure 1 shows the local energy, $H\psi_{trial}/\psi_{trial}$, averaged over the walkers at each step of a DMC calculation. The number of walkers fluctuated near 40 000 during these runs. Figure 1 illustrates the sensitivity of results to the quality of the guiding function chosen. We employ guiding functions, described in detail below, that have been optimized in prior variational Monte Carlo (VMC) calculations. The trial function, used to produce the plot in Figure 1a yields a VMC estimate of the ground-state energy 1627 cm^{-1} above the exact value. Our best trial function produces a variational energy expectation value that is 553 cm^{-1} above the true ground state. It is apparent that the guiding function makes an enormous difference in the fluctuations of the local energy, as depicted in Figure 1, and consequently in the statistical errors of our final result.

Although functions as simple as a multidimensional Gaussian have been used for the trial wave function,[73,74] we chose a relatively complex and flexible form of the guiding function to obtain a precise estimate of the zero-point energy of $H_5O_2^+$. Other authors have noted that the choice of internal coordinates and form of the trial wave function affects the quality of the trial wave function.[54] The trial wave function was optimized for the OSS3 model,[6,64] but we expect that this form can also be applied to more accurate potential energy surfaces for $H_5O_2^+$ as they become available. A simple *ansatz* for the trial wave function, such as a Gaussian, simplifies the calculation of the local energy. When the trial function is more flexible, calculation of analytic expressions for the local energy and quantum force, $\nabla \ln|\psi_{trial}|^2$, becomes exceedingly complex. To handle this difficulty, a symbolic algebra program[75] is employed to automatically generate FORTRAN code to calculate the local energy and quantum force. The trial wave function used in

TABLE 2: Coupling Terms Used for $H_5O_2^+$ Guiding Function

term	characterization
$\alpha_1[(d_{OH_1}-\alpha_2)(d_{HH_a}-\alpha_3)+(d_{OH_2}-\alpha_2)(d_{HH_a}-\alpha_3)+(d_{OH_3}-\alpha_2)(d_{HH_b}-\alpha_3)+(d_{OH_4}-\alpha_2)(d_{HH_b}-\alpha_3)]$	OH−HH coupling
$\alpha_4(d_a-d_b)^2(R-\alpha_5)$	*R*, central proton stretch coupling
$\alpha_6(d_a-d_b)(d_{HH_a}+d_{HH_b}-2\alpha_3)$	water HH, central proton stretch coupling
$\alpha_7(d_a-d_b)(\omega_a+\omega_b-2\alpha_8)$	wag, central proton stretch coupling
$\alpha_9(R-\alpha_5)(d_{OH_1}+d_{OH_2}+d_{OH_3}+d_{OH_4}-4\alpha_2)$	*R*, OH coupling
$\alpha_{10}(R-\alpha_5)(\omega_a+\omega_b-2\alpha_8)$	water wag, *R* coupling
$\alpha_{11}[(d_1-\alpha_{12})(d_3-\alpha_{12})+(d_2-\alpha_{12})(d_4-\alpha_{12})]$	hydronium bending coupling
$(d_{OH_1}-\alpha_{13})[\alpha_{14}(d_1-\alpha_{12})+\alpha_{15}(d_3-\alpha_{12})]+(d_{OH_2}-\alpha_{13})[\alpha_{15}(d_1-\alpha_{12})+a_{14}(d_3-\alpha_{12})]+(d_{OH_3}-\alpha_{13})[\alpha_{14}(d_2-\alpha_{12})+\alpha_{15}(d_4-\alpha_{12})]+(d_{OH_4}-\alpha_{13})[\alpha_{15}(d_2-\alpha_{12})+\alpha_{14}(d_4-\alpha_{12})]$	OH, hydronium bending coupling
$(d_a-\alpha_{16})(d_1+d_3-2\alpha_{12})+(d_b-\alpha_{16})(d_2+d_4-2\alpha_{12})$	central proton stretch, hydronium bending coupling

Figure 1b required 7572 lines of code automatically generated by the symbolic algebra program after input of the analytic form of the guiding function.

Our labeling scheme for $H_5O_2^+$ in its C_2 equilibrium geometry is shown in Figure 2. The oxygens and central proton define the *yz* plane. The outer hydrogens do not lie in the *yz* plane. Although the OSS3 model permits interchange of the outer and central hydrogen atoms, such rare events, which give rise to small tunnel splittings, were not allowed by our trial wave function. Wales[15] has reported that the barrier to this motion is 4555 cm^{-1}, an order of magnitude larger than the barriers for other inversion and internal rotational motions, all of which are allowed in our calculations. The trial wave function is expressed in terms of the internal coordinates specified in Table 1. The trial wave function is of the form

$$\psi_{\text{trial}} \propto e^{-f} \tag{1}$$

where *f* is a sum of effective potentials, or Jastrow factors,[76] which depend on the coordinates defined in Table 1. The actual form of the function *f* used in our study is

$$f = v_1(d_a)+v_1(d_b)+v_2(R)+v_3(z^2)+\sum_{i=1}^{4}v_4(d_{OH_i})+v_5(d_{HH_a})+v_5(d_{HH_b})+v_6(\omega_a)+v_6(\omega_b)+v_7(\Theta_{ab})+v_8(\Theta_a)+v_8(\Theta_b)+\sum_{i=1}^{4}v_9(d_i)+v_{10}(|\mathbf{r}_B-\mathbf{r}_3|)+v_{10}(|\mathbf{r}_C-\mathbf{r}_3|)+\text{coupling terms} \tag{2}$$

where

$d_i = |\mathbf{r}_{i+3}-\mathbf{r}_3|$

(distances between central and outer hydrogens)

$i = 1, 2, 3, 4,$

$$v_j(x_\mu) = \frac{1}{2}K_j^2(x_\mu - x_{\mu j}^0)^2 \quad j \le 2 \tag{3}$$

$$v_j(x_\mu) = \frac{1}{2}K_j(x_\mu - x_{\mu j}^0)^2 + \frac{1}{3}L_j(x_\mu - x_{\mu j}^0)^3 + \frac{1}{4}M_j^2(x_\mu - x_{\mu j}^0)^4 \quad j < 2$$

and the coupling terms are specified in Table 2.

A trial wave function with 34 parameters was optimized by minimizing the energy in VMC calculations. The VMC energy estimate depends on a sample of configurations representative of ψ_{trial}. Optimization techniques, such as conjugate gradient, which allow large changes in parameter values upon each iteration proved to be unwieldy in this situation. When the parameters of ψ_{trial} change significantly, the representation of $|\psi_{\text{trial}}|^2$ by the sample of configurations deteriorates, and the VMC energy estimate, even with reweighting,[72] is no longer meaningful. The simulated annealing method,[77] with frequent updates of the sample from $|\psi_{\text{trial}}|^2$, emerged as an effective procedure for variational optimization. Diffusion Monte Carlo was performed using a series of different imaginary time steps, with the optimized trial wave function of eq 1 as the guiding function. The zero-point energy was obtained by $\tau \to 0$ extrapolation of the results as shown in Figure 3. Our estimate of ZPE for the OSS3 potential model is 12 218.7 (±0.6) cm^{-1}. Statistical errors were estimated using the blocking method described by Flyvbjerg and Petersen.[78]

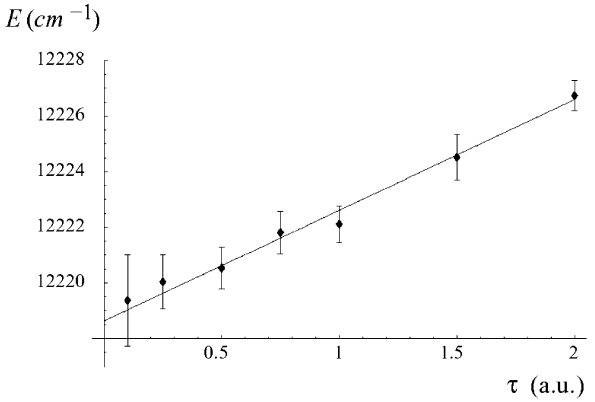

Figure 3. Extrapolation of the DMC ground-state energy to zero imaginary time step τ. We attempted to fit the data to both $\tau^{1/2}$ and τ and found that the linear fit gave the best representation of the data.

Analysis of the DMC Wave Function. Configurations generated by DMC sampling are representative of the probability distribution, $P = \psi_{\text{trial}}\Phi$, where Φ is the exact ground-state wave function, distinct from the desired average over the true wave function weighted by $|\Phi|^2$. Methods to directly calculate averages are available,[79] but require significant overhead. A convenient approximation to the desired averages, which is used in this study, is to weight configurations by the distribution

$$2P - |\psi_{\text{trial}}|^2 \tag{4}$$

which is the true probability function up to order $\delta \equiv \Phi - \psi_{\text{trial}}$ (i.e., with errors entering at order δ^2). This follows because

$$\Phi^2 = (\psi_{\text{trial}}+\delta)^2 = 2P - \psi^2{}_{\text{trial}} + \delta^2 \tag{5}$$

The validity of the approximation in eq 4 depends on the quality of the trial wave function. The flexible form of our ψ_{trial} yields accurate averages, as evidenced by the fact that $|\psi_{\text{trial}}|^2$ itself is already quite close to the approximation of eq 4, as confirmed in Figure 4.

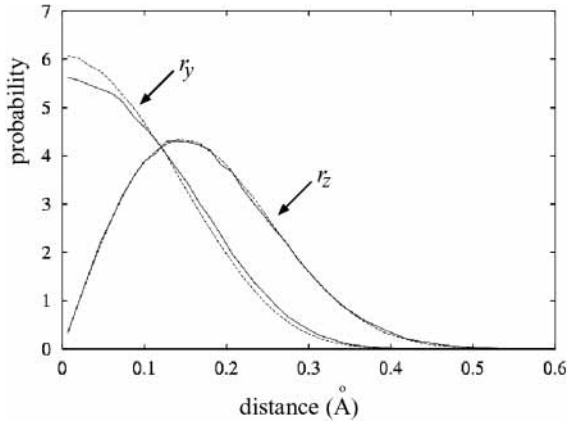

Figure 4. Probability distribution for deviation of the central proton from the midpoint of the oxygen−oxygen bond. The solid lines are the probability, $2P - |\psi_{trial}|^2$, estimated using the importance sampling function $P = \psi_{trial}\Phi$ and the trial wave function. (See the discussion following eq 4.) The dashed lines are the probabilities from the variational wave function, $|\psi_{trial}|^2$. The closeness of the two probability estimates confirms the accuracy of our trial wave function and expression 4 for the probability.

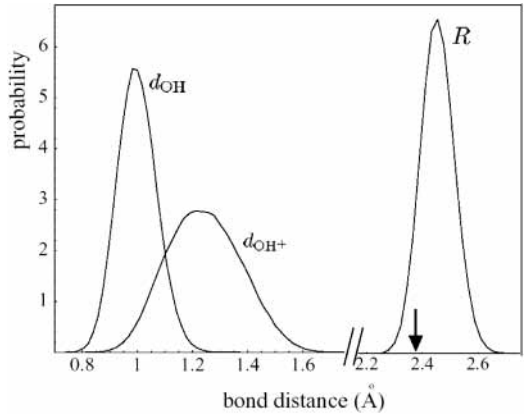

Figure 5. Distribution of inner (d_{OH}^+, solid line) and outer (d_{OH}, dashed line) oxygen−hydrogen bond lengths and the oxygen−oxygen distance (R) in the $H_5O_2^+$ ion as it undergoes zero-point fluctuations.

Probability distributions for the deviation of the central proton from the midpoint of the two molecular oxygens (Figure 4) clearly show the strength of zero-point fluctuations at 0 K. The average deviation of the central proton in the *z*-direction, perpendicular to the inter-oxygen axis, is 0.17 Å, in comparison with a deviation of 0.073 Å at the equilibrium structure. The estimated standard deviation is 0.09 Å, which is already more than 50% of the average distance itself. The width of the distribution in Figure 4 rather resembles that of path integral simulations by Cheng et al.[80] that explored the quantum fluctuations of the $H_5O_2^+$ ion at 150 K on the somewhat different potential surface given by their ab initio molecular dynamics methodology. This indicates that most of the fluctuations they observed stem from zero-point motion, and agrees with their analysis of the path integral imaginary time correlation function which pointed to ground state dominance. While Cheng et al. found significant differences between classical and quantum behavior at 150 K, Tuckerman et al., using similar path integral methodology, found less striking difference between quantum and classical distributions at 300 K.[81]

Figure 5 depicts the distribution of inner (d_{OH}^+, solid line) and outer (d_{OH}, dashed line) oxygen−hydrogen bond lengths. The standard deviation for fluctuations of the central proton along the oxygen−oxygen axis is 0.13 Å, much greater than

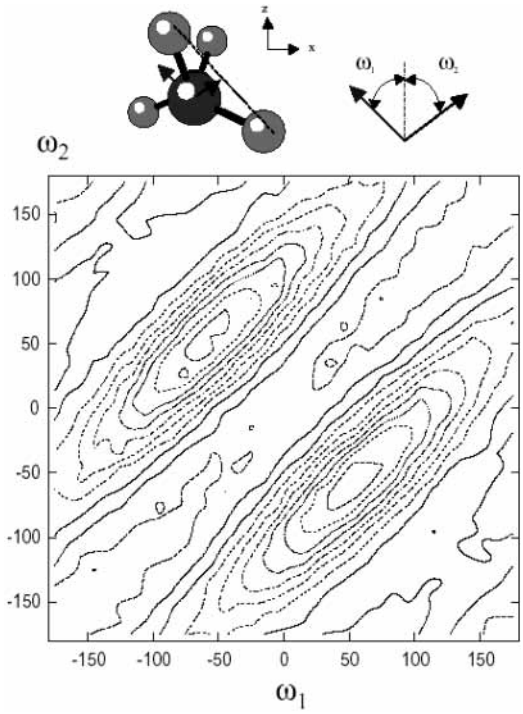

Figure 6. Joint probability distribution of the water−water torsion angles. The angle ω_1 and ω_2 are defined in terms of molecular bisectors, the average of two oxygen−hydrogen vectors for outer hydrogens bound to the same oxygen. Then, ω_1 and ω_2 are the dihedral angles between planes containing a molecular bisector and the oxygen−oxygen vector, and a second plane containing the two oxygens and the middle hydrogen. The maximum contours [small ellipsoids at roughly (−50, 50) and (50, −50)] are drawn where the probability has the value 2.7×10^{-5}. Succeeding contours are drawn at values lowered by increments of 3×10^{-6}.

bond length fluctuations of the outer OH bonds. The average d_{OH} is slightly larger than the equilibrium value by 0.03 Å. Another noticeable feature of zero-point quantum effect is the elongation of the distance between two water oxygens, as shown in Figure 5. The arrow in Figure 5 designates the inter-oxygen distance from the equilibrium structure.

In Figure 6, we plot the distribution of torsion angles of the two outer water molecules. The torsion angles are defined from the molecular bisector of the waters to the *z*-axis established by the deviation of the central proton from the midpoint of the oxygen−oxygen bond, the *z*-axis indicated in Figure 2. The two maxima of Figure 6 locate two local minima of C_2 symmetry on the potential surface that are mirror images of each other. Lines of slope +1 in Figure 6 are lines of constant $\omega_2 - \omega_1$, the torsion angle difference between the two waters. There is a relatively strong tendency for the waters to be separated by $\sim\pm 110°$. Lines of slope −1 are lines of constant $\omega_2 + \omega_1$, which describes the average torsion angle of the waters relative to the central hydrogen. This coupling is weak, but still evident in Figure 6.

In their reduced dimensionality calculations, Vener et al. chose the oxygen−oxygen distance and the three coordinates for the central hydrogen for explicit calculation.[32] Working in an adiabatic approximation, their effective potential surface for these four active coordinates is the full potential minimized over all other coordinates except for the torsion angles, which are constrained to have a fixed value of $\omega_1 - \omega_2$. This approximation will be accurate in the opposing limits of either highly restricted motion in this coordinate, or nearly free, motion. From Figure 6, it is evident that the behavior of the $H_5O_2^+$ ion in our calculations lies somewhere between these two limits.

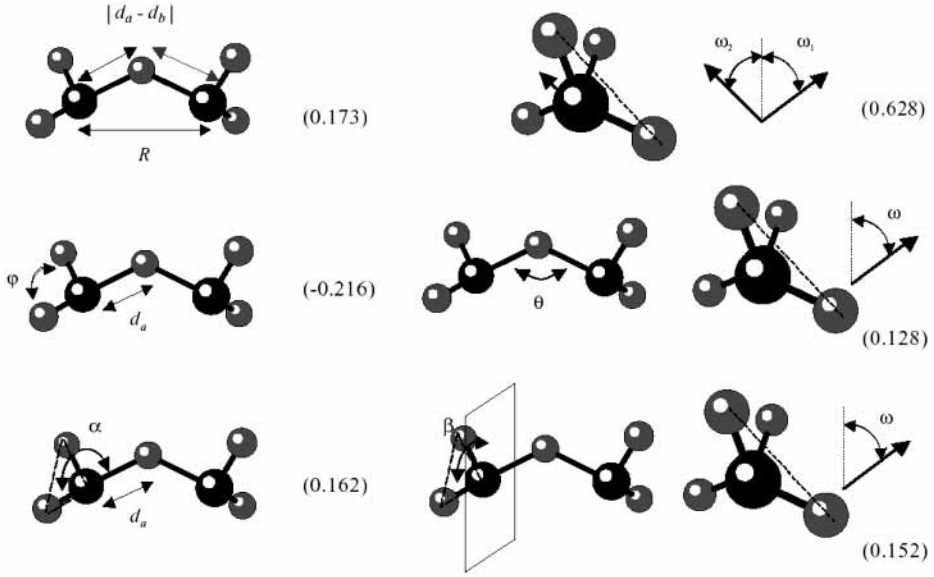

Figure 7. Correlation coefficients, as defined in eq 6, with figures illustrating the nature of the coordinates involved.

Assessing the degree of coupling between internal coordinates gives important information needed to benchmark more approximate treatments of the system and indicates which couplings must be included. The full zero-point probability distribution from DMC calculations allows identification of coordinates whose zero-point fluctuations are strongly correlated. We accumulated normalized correlation coefficients among pairs of internal coordinates, defined as

$$c_{ij} \equiv \frac{\sigma_{ij}^{\ 2}}{\sigma_{ii}\sigma_{jj}} = \frac{\langle (x_i - \langle x_i \rangle)(x_j - \langle x_j \rangle) \rangle}{\sqrt{\langle (x_i - \langle x_i \rangle)^2 \rangle \langle (x_j - \langle x_j \rangle)^2 \rangle}} \qquad (6)$$

between two coordinates x_i and x_j. Some of the larger correlation coefficients are depicted in Figure 7.

To qualitatively interpret the importance of those correlations on the estimation of vibrational frequencies in possible reduced dimensionality calculations, we studied the analogous situation in a simplified model. We examine the correlation introduced by the force constant k_{ij} between two harmonic coordinates in the Hamiltonian,

$$-\frac{\hbar^2}{2m_i}\frac{d^2}{dx_i^{\ 2}} - \frac{\hbar^2}{2m_j}\frac{d^2}{dx_j^{\ 2}} + \frac{1}{2}k_{ii}x_i^{\ 2} + \frac{1}{2}k_{jj}x_j^{\ 2} + k_{ij}x_i x_j \qquad (7)$$

It is an elementary exercise to express the frequencies and ground state wave function in terms of the parameters introduced in eq 7. The correlation coefficient introduced in eq 6 are extracted from the square of the wave function. We expand the frequencies and moments to leading order in k_{ij}, and then use the moments σ_{ii}, σ_{jj} and σ_{ij} to eliminate k_{ij} and the masses from the frequency. Finally, we can express the fractional shift in the frequencies in terms of the correlation coefficient and the zero-order frequencies $\omega_n^0 \equiv \sqrt{\frac{k_{nn}}{m_n}}$, $n = i,j$.

$$\frac{\Delta\omega_{ij}}{\omega_i^0 - \omega_j^0} = \frac{1}{2}\left(\frac{\omega_i^0 + \omega_j^0}{\omega_i^0 - \omega_j^0}\right)^2 c_{ij}^{\ 2} + \ldots \qquad (8)$$

In the above equation, the total shift of the two levels from their zero-order values, $\Delta\omega_{ij}$, is given by

$$\Delta\omega_{ij} = (\omega_i - \omega_i^0) - (\omega_j - \omega_j^0) \qquad (9)$$

where ω_i and ω_j are the frequencies that reduce to ω_i^0 and ω_j^0, respectively, as $k_{ij} \rightarrow 0$.

Since the fractional shift in frequencies depends on the square of the correlation coefficient, it may seem that the correlations identified in Figure 7 may have small effect. However, c_{ij}^2 in eq 8 is multiplied by a factor which tends to be rather large. For example, if the splitting between the zero-order frequencies is as small as 40% of their average, then a correlation coefficient of magnitude 0.2 indicates that inclusion of the coupling k_{ij} will increase the frequency splitting by 50%. If the zero-order levels are even closer, then the shift will be even more dramatic. Hence, the correlation coefficients reported in Figure 7 indicate significant couplings among internal coordinates.

Several of the examples in Figure 7 have a clear physical interpretation. The first example of correlation in Figure 7, positive correlation between $|d_a - d_b|$ and R, captures the tendency for $H_5O_2^+$ to behave like an asymmetric hydronium−water pair (large $|d_a - d_b|$) when the two oxygens fluctuate beyond their equilibrium separation (large R). Moving down the first column of Figure 7, the negative correlation between the bend angle ϕ and d_a reflects a related effect: As the central hydrogen deviates from the midpoint of the oxygen−oxygen bond, the unit furthest from the central hydrogen behaves like a water molecule, while the rest of the molecule behaves like H_3O^+. This is reflected in a negative correlation between ϕ and d_a since, for large values of d_a, the bond angle approaches that of water, which is smaller than the bond angle in hydronium. Strong zero-point fluctuations toward asymmetric H_3O^+- H_2O character also explain the overlap of the d_{OH}^+ and d_{OH} oxygen−hydrogen distances in Figure 5. When the $H_5O_2^+$ ion is in an asymmetric configuration, one of the d_{OH}^+ distances is expected to be comparable to d_{OH}. The last four examples in Figure 7 indicate that strong correlations exist among the various wagging, torsion and bending angles in $H_5O_2^+$.

III. MULTIMODE Calculations

MULTIMODE is a general code which performs quantum rovibrational energy calculations of polyatomic molecules. The

code is based on the full Watson Hamiltonian, which is an exact Hamiltonian for rovibrational motion, given in terms of mass-scaled normal modes, Q_i.[82,83] The code has been described and tested previously.[60−63] In recent applications to tunneling splittings in NH_3 and H_3O^+, modifications of the methodology were made to accurately describe the delocalized motion in a multidimensional double well.[84−87] These modifications, which are briefly described below, were used in the present calculations. A key feature of MULTIMODE that makes calculations of fairly large molecules feasible is the representation of the full N-mode potential by an exact hierarchical series of mode-coupling terms:

$$V(Q_1, Q_2, ..., Q_N) = \sum_i V_i^{(1)}(Q_i) + \sum_{ij} V_{ij}^{(2)} ij\,(Q_i,Q_j) + \sum_{ijk} V_{ijk}^{(3)}(Q_i,Q_j,Q_k) + \sum_{ijkl} V_{ijkl}^{(4)}(Q_i, Q_j, Q_k, Q_l) + ...$$

where the *one-mode representation* of the potential contains only $V_i^{(1)}(Q_i)$ terms, i.e., the potential along cuts of the normal coordinates; the *two-mode representation* of the potential contains these terms plus the $V_{ij}^{(2)}(Q_i,Q_j)$ terms where any pair of normal modes vary, etc. In the present calculations, for which there are 15 modes, the series is truncated at the four-mode representation. This representation of the potential makes the dimensionality of integrals involving V at most four, for any number of normal coordinates.

Eigenvalues and eigenfunctions of the Watson Hamiltonian are obtained using the "VCI" approach. All of these begin with a vibrational self-consistent field (VSCF) Hamiltonian for the ground vibrational state. The CI method, denoted VCI, uses the "virtual" orthonormal basis of eigenfunctions of the single VSCF Hamiltonian for the ground state. The size of the VCI Hamiltonian matrix grows nonlinearly with the size of the molecule, and the numerical evaluation of the matrix elements can become very time-consuming. Thus, numerical quadratures are done using a reduced set of "potential optimized" quadratures, as described in detail elsewhere.[61]

To use MULTIMODE, a reference stationary geometry, at which a normal-mode analysis is done, must be specified. For $H_5O_2^+$, where large amplitude motion can occur, we chose for the reference geometry a second-order saddle point with the proton midway between the two O atoms and in a linear arrangement. During geometry optimization for the reference point, all other degrees of freedom are allowed to vary freely except the central proton which is fixed at the midpoint of O···O. This choice permits a description of the large amplitude motion of the proton between the equivalent two minima of $H_5O_2^+$, which correspond to the two maxima of the probability distribution observed in Figure 6.

The normal coordinates were obtained for this stationary point as well as for one of the minima. The harmonic frequencies and C_2 symmetries are given in Table 3. These results are in very good agreement with those of Valeev and Schaefer.[16] As depicted in Figure 8a, the imaginary mode Q_1 describes the central proton transfer between two oxygens, which is coupled with the vibrations of the two H_2O fragments in $H_3O^+\cdots H_2O$ formation, as is clear from Figure 8a. The other imaginary mode Q_2, see Figure 8b, represents the proton oscillating along a direction perpendicular to the O···H···O line and C_2 axis, accompanied by anticlockwise $-OH_2$ rotations. Cuts of the potential surface along each of the two imaginary modes reveal a pair of minima on either side of the reference point. Minima along these one-dimensional cuts are not true local minima of the potential surface, and, in particular, not the two equivalent global minima discussed above. Along the 1-D potential cut of Q_1, the barrier connecting the two local minima is quite small, only 0.99 cm^{-1}. The bottom of the potential curve along the Q_2 1-D cut is even flatter, and the barrier height is only 0.16 cm^{-1}. Figure 9 plots the Q_1-Q_2 potential contour spanned around the reference geometry, while all the other 13 modes are held fixed at zero. It clearly demonstrates the boxlike character of the potential in these two modes.

The potential at our reference geometry is 97.236 cm^{-1}, relative to the global minima. This small value is another indication that the proton motion, even in the ground vibrational state, will be delocalized over the two equivalent global minima.

TABLE 3: C_2 Symmetries and Harmonic Frequencies of 15 Normal Modes at the Global Minimum and the Second-Order Saddle Point Used in MM4.6 Calculations (in cm^{-1})

	ref[a]		global minimum			2nd-order saddle point		
mode	C_2 sym	freq	mode	C_2 sym	freq	mode	C_2 sym	freq
ω_8	A	241	1	A	178	1	B	198i
ω_{15}	B	296	2	B	182	2	B	82i
ω_7	A	481	3	A	552	3	B	538
ω_6	A	561	4	B	552	4	A	548
ω_{14}	B	577	5	A	584	5	A	571
ω_5	A	650	6	A	688	6	A	674
ω_{13}	B	794	7	B	857	7	B	877
ω_{12}	B	1505	8	B	1486	8	B	1471
ω_4	A	1596	9	A	1505	9	A	1512
ω_3	A	1746	10	A	1716	10	A	1701
ω_{11}	B	1787	11	B	1871	11	B	1881
ω_{10}	B	3766	12	B	3700	12	B	3716
ω_2	A	3806	13	A	3796	13	A	3813
ω_9	B	3854	14	B	3883	14	B	3900
ω_1	A	3868	15	A	3894	15	A	3912

[a] B-CCD(T)/TZ2P results, at the minimum, from ref 16.

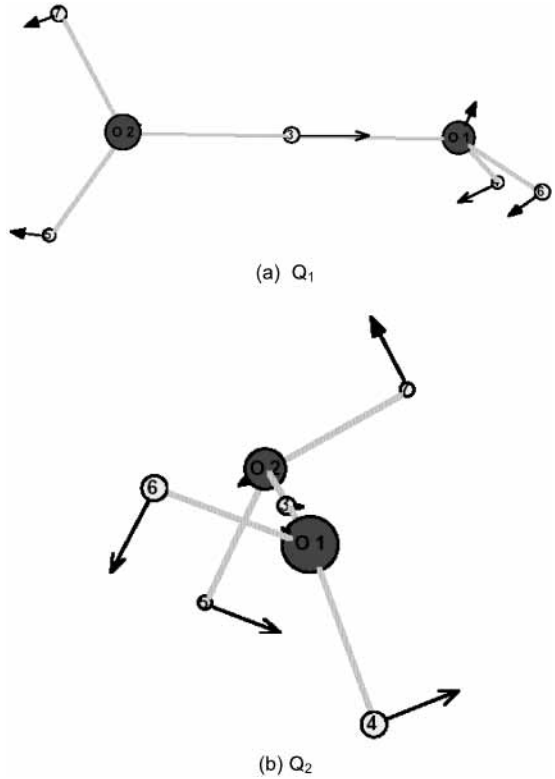

Figure 8. Two imaginary vibrational modes at the second-order saddle point, in which the O···H···O fragment is linear. (a) Mode Q_1, the proton-transfer mode. (b) Mode Q_2, the central proton slightly oscillating perpendicular to the O···H···O fragment, coupled with terminal $-OH_2$ rotations.

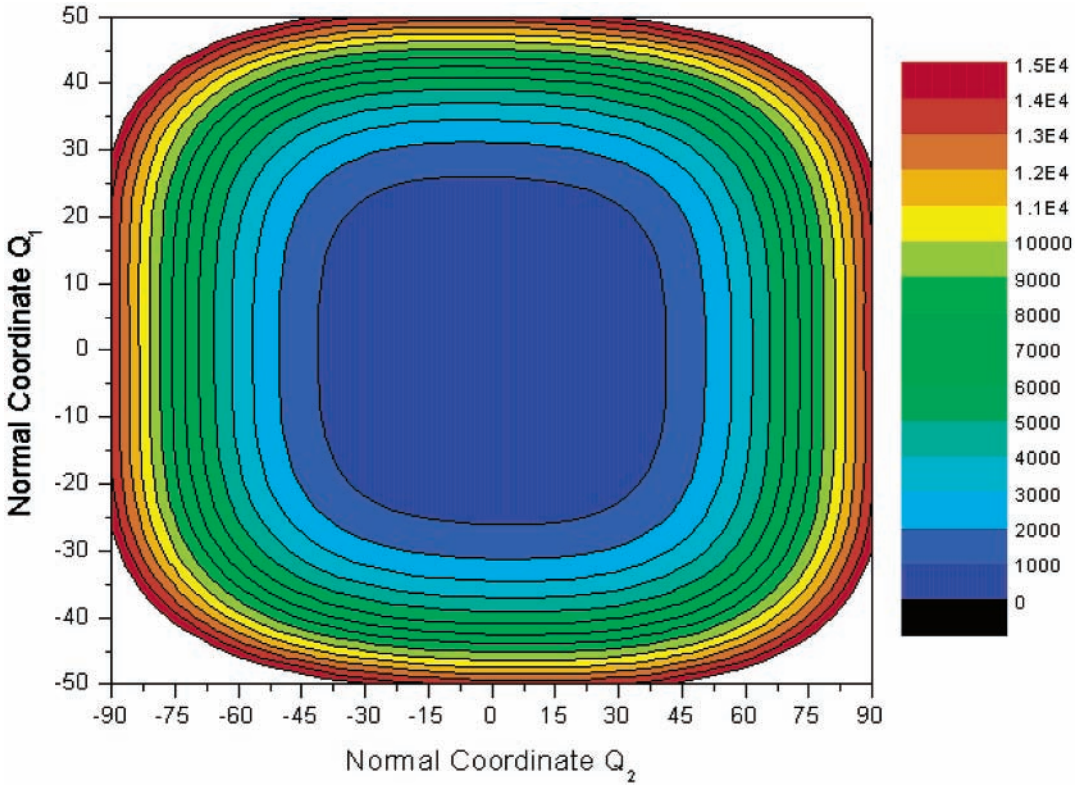

Figure 9. Equipotential contour plot of the $H_5O_2^+$ OSS3 potential (cm^{-1}) in the normal modes Q_1(proton-transfer mode) and Q_2(proton oscillating mode) with all other modes held fixed at zero.

There would be no vibrational state splittings caused by the central proton transfers.

In the MM4.6 calculations, new features specially designed for the problems involving saddle points,[84–87] have been utilized. These new features have been described previously,[84,85] e.g., the numerical bases consist of symmetric or asymmetric functions (with respect to $Q_1 = Q_2 = 0$) that span both minima. Instead of taking direct cuts of the potential along each mode with other modes held fixed at zero, the one-dimensional potentials of modes Q_3, Q_4, and Q_5 were optimized with respect to Q_2, for each value of Q_j, $j = 3-5$, the potential was minimized with respect to Q_2. For strongly coupled modes, such minimizations ensure better descriptions of the contracted basis functions over large displacements. Accordingly, large bases of primitive functions and large number of quadratures points are required. The numerical basis for the three modes was obtained using a relatively large primitive harmonic-oscillator basis defined by the harmonic frequencies given in Table 3.

For modes Q_3, Q_4 and Q_5, seven numerical basis functions were contracted from a primitive basis of 23 harmonic-oscillator functions. For other modes, seven numerical basis functions were contracted from 13 primitive harmonic-oscillator functions. Techniques used to determine optimized quadratures points have been described elsewhere.[61] Since there are 15 degrees of freedom, an excitation-unlimited VCI is still far beyond our computational capabilities, Hamiltonian matrices of different sizes have been constructed and diagonalized so that the trend between CI matrix size and vibrational state convergences could be established. Six VCI calculations are reported in the next section, using the same 1-D bases as mentioned above. Four of them use a four-mode representation of the potential, denoted as 4MR-I through 4MR-IV. However, the other two VCI calculations used a 3-mode representation, denoted as 3MR-I, 3MR-II. The largest calculation, 4MR-IV, used number of basis functions of order 38540 (for A symmetry) and 37776 (for B symmetry).

TABLE 4: Zero-Point Energies (in cm^{-1}) Relative to the Global Minimum for the Indicated VCI Basis

	3MR-I	3MR-II	4MR-I	4MR-II	4MR-III	4MR-IV
size of CI	408	7304	6261	15 593	25 587	38 540
matrices	408	7142	6240	15 648	25 894	37 776
VSCF ZPE	12775.0	12778.1	12769.4	12768.9	12768.9	12753.4
VCI ZPE	12403.3	12313.4	12342.5	12320.6	12312.7	12309.9

[a] The DMC zero-point energy is 12218.7 (±0.6) cm^{-1}. One of the two CI matrices refers to A symmetry, and the other is for B symmetry.

Zero-Point Energy. The zero-point energies of $H_5O_2^+$, calculated by MM4.6, are presented in Table 4 for various VCI bases. We also give the VSCF energies in that table. As seen, the VSCF results are roughly 500 cm^{-1} above the accurate DMC result. (Recall, also that the best variational trial wave function has a similar error.) The VCI ZPE appears to be converging to a value of 12310 cm^{-1}, about 92 cm^{-1} above the DMC value. Since the reference geometry in the MULTIMODE calculations is not at the global minimum, it is important to determine whether that minimum is contained in the NMR grids. We did investigate this and determined that the global minimum is contained in the three- and (therefore) the four-mode grids, but not in the two-mode grids. Thus, this possible shortcoming of the choice of reference geometry does not appear to be of concern for three- and four-mode calculations.

We also investigated using a minimum as the reference geometry. Large 4MR VCI were done with this choice, and the resulting ZPE is 12346 cm^{-1}. This result is slightly higher than the one obtained using the second-order saddle point as the reference geometry.

The MM zero-point energy appears to be fairly well converged with the respect to the level of mode-coupling;

TABLE 5: Fundamentals of 15 Modes Calculated by MM4.6 3MR and 4MR VCI, Related to Respective ZPEs, Where 4MR-IV Values Are Taken as the Closest to Converged (in cm^{-1})

mode	3MR-II	4MR-IV
1	599	516
2	491	310
3	738	583
4	751	590
5	674	569
6	715	564
7	822	914
8	1529	1369
9	1530	1380
10	1832	1646
11	1747	1809
12	3422	3319
13	3650	3427
14	3527	3468
15	3544	3472

however, the 4MR ZPE is 90 cm^{-1} above the DMC result. This raises the possibility that either a higher level of mode coupling is needed or that the grid used in the MM calculations is not sufficiently large. We plan to investigate both of these possibilities in the future, by doing 5MR calculations and also doing MM calculations with a "Reaction Path Hamiltonian" (RPH) as described elsewhere.[86,88] The RPH approach can in principle describe vibrational motions on a potential with multiple minima.

Vibrational Fundamentals. For each symmetry of Hamiltonian matrices, the eigenvectors for the 500 lowest vibrational states were obtained along with their corresponding eigenvalues. The leading CI coefficients and corresponding bases of VSCF eigenfunctions that are contained in each final VCI state are also found and used to assign states. The assignment based on these coefficients can be problematic due to large mixing in the basis. This mixing is due to the floppy motions in $H_5O_2^+$. The vibrational fundamentals calculated from the largest 3MR-II and 4MR-IV are given in Table 5. The 4MR-IV results are taken as closer to converged fundamental energies. In contrast to the ZPE, there are significant differences between the 3MR and 4MR fundamentals.

The four OH-stretch fundamentals are of special interest since two have been determined experimentally.[45,46] Note the large differences with the harmonic frequencies at either the saddle point or the minimum reference geometry. The calculations show a large red-shift in the OH-stretch fundamentals relative to the harmonic frequencies in qualitative agreement with experiment. However, acceptable quantitative agreement with experiment is lacking. We have done preliminary five-mode calculations of the fundamentals and it appears that the 4MR results are converged to within roughly 10 cm^{-1}. This suggests that the potential is the major source of disagreement with experiment for the two experimentally reported fundamentals. We plan to investigate this in the future by reexamining the fit to the original ab initio energies[6,64] and also doing new, higher level ab initio calculations. We also plan to redo the vibrational calculations with the "Reaction Path" version of MULTIMODE[86,88] to check the accuracy of the present MULTIMODE calculations.

IV. Summary

Two full-dimensional quantum calculations of the vibrational energies of $H_5O_2^+$ are presented here, using the OSS3(p) potential. A highly accurate zero-point energy is computed in a diffusion Monte Carlo study. A detailed analysis of the DMC wave function, including population profiles and correlations, has been discussed. MULTIMODE vibrational self-consistent field and configuration interaction calculations have been carried out with a consistent set of increasing Hamiltonian bases for three and four-mode coupling. The agreement between the DMC ZPE and MM4.6 CI ZPEs is good, especially considering the difficulties posed by this weakly bonded cation. Fundamental vibrational frequencies obtained from MULTIMODE have been reported as several levels of approximation, and convergence trends have been discussed.

Acknowledgment. J.M.B. and S.C. thank the U.S. Office of Naval Research (Grants ONR-N00014-01-1-0235 and N00014-02-1-0629) for financial support of this work. H.M.C. and S.J.S. acknowledge NSF Grant No. CHE-0109243 for support and the Ohio Supercomputer Center for resources needed to perform the DMC calculations reported here. Finally, it is a pleasure to dedicate this paper to Don Kouri.

References and Notes

(1) Kebarle, P.; Searles, S. K.; Zolla, A.; Scarborough, J.; Arshadi, M. *J. Am. Chem. Soc.* **1967**, *89*, 6393.
(2) Cunningham, A. J.; Payzant, J. D.; Kebarle, P. *J. Am. Chem. Soc.* **1972**, *94*, 7627.
(3) Meot-Ner, M.; Field, F. H. *J. Am. Chem. Soc.* **1977**, *99*, 998.
(4) Lau, Y. K.; Ikuta, S.; Kebarle, P. *J. Am. Chem. Soc.* **1982**, *104*, 1462.
(5) Magnera, T. F.; David, D. E.; Michl, J. *Chem. Phys. Lett.* **1991**, *182*, 363.
(6) Ojamäe, L.; Shavitt, I.; Singer, S. J. *Int. J. Quantum Chem., Quantum Chem. Symp.* **1995**, *29*, 657.
(7) Yamabe, S.; Minato, T. *J. Chem. Phys.* **1984**, *80*, 1576.
(8) Frish, M. J.; Del Bene, J. E.; Binkley, J. S.; Schaefer, H. F., III. *J. Chem. Phys.* **1986**, *84*, 2279.
(9) Lee, E. P. F.; Dyke, J. M. *Mol. Phys.* **1991**, *73*, 375.
(10) Xie, Y.; Remington, R. B.; Scheaefer, H. F., III. *J. Chem. Phys.* **1994**, *101*, 4878.
(11) Pudzianowski, A. T. *J. Chem. Phys.* **1995**, *102*, 7761.
(12) Tuma, C.; Boese, A. D.; Handy, N. C. *Phys. Chem. Chem. Phys.* **1999**, *1*, 3939.
(13) Newton, M. D.; Ehrenson, S. *J. Am. Chem. Soc.* **1971**, *93*, 4971.
(14) Olovsson, I. *J. Chem. Phys.* **1968**, *49*, 1063.
(15) Wales, D. J. *J. Chem. Phys.* **1999**, *110*, 10403.
(16) Valeev, E. F.; Scheaefer, H. F., III. *J. Chem. Phys.* **1998**, *108*, 7197.
(17) Wei, D.; Salahub, D. R. *J. Chem. Phys.* **1994**, *101*, 7633.
(18) Mijoule, C. *Chem. Phys. Lett.* **1993**, *208*, 364.
(19) Barone, V.; Orlandini, L.; Adamo, C. *Chem. Phys. Lett.* **1994**, *231*, 295.
(20) Liao, H.-Y.; Chu, S.-Y. *Int. J. Quantum Chem.* **2002**, *90*, 507.
(21) Auer, A. A.; Helgaker, T.; Klopper, W. *Phys. Chem. Chem. Phys.* **2000**, *2*, 2235.
(22) Salvador, P.; Duran, M.; Dannenberg, J. J. *J. Phys. Chem. A* **2002**, *106*, 6883.
(23) Scuseria, G. E.; Scheiner, A. C.; Lee, T. J.; Rice, J. E.; Schaefer, H. F., III. *J. Chem. Phys.* **1986**, *86*, 2881.
(24) Muguet, F. F. *J. Mol. Struct.: THEOCHEM* **1996**, *368*, 173.
(25) Klein, S.; Kochanski, E.; Strich, A.; Sadlej, A. J. *J. Phys. Chem. A* **1997**, *101*, 4799.
(26) Pudzianowski, A. T. *J. Chem. Phys.* **1995**, *102*, 8029.
(27) Platts, J. A.; Laidig, K. E. *J. Phys. Chem.* **1995**, *99*, 6487.
(28) Ichihashi, M.; Yamabe, J.; Murai, K.; Nonose, S.; Hirao, K.; Kondow, T. *J. Phys. Chem.* **1996**, *100*, 10050.
(29) Hirao, K.; Fujikawa, T.; Konishi, H.; Yamabe, J. *Chem. Phys. Lett.* **1984**, *104*, 184.
(30) Williams, G. R. J. *J. Mol. Struct.: THEOCHEM* **1986**, *138*, 333.
(31) Kollman, P. A.; Allen, L. C. *J. Am. Chem. Soc.* **1970**, *92*, 6101.
(32) Vener, M. V.; Kuhn, O.; Sauer, J. *J. Chem. Phys.* **2001**, *114*, 240.
(33) Vener, M. V.; Sauer, J. *Chem. Phys. Lett.* **1999**, *312*, 591.
(34) Minichino, C.; Voth, G. A. *J. Phys. Chem. B* **1997**, *101*, 4544.
(35) Zundel, G.; Frish, M. J. In *The Chemical Physics of Solvation*; Dogonadze, R., Kalman, E., Kornyshev, A. A., Ulstrup, J., Eds.; Elsevier: Amsterdam, 1986; Vol. 2, Chapter 2.
(36) Essayem, N.; Holmqvist, A.; Gayraud, P. Y.; Vedrine, J. C.; Taarit, Y. B. *J. Catal.* **2001**, *197*, 273.
(37) Yukhnevich, G. V.; Tarakanova, E. G.; Mayorov, V. D.; Librovich, N. B. *J. Mol. Struct.* **1992**, *265*, 237.
(38) Sato, S.; Ido, A. *J. Chem. Phys.* **2000**, *113*, 7453.

(39) Jones, D. J.; Roziere, J.; Penfold, J.; Tomkinson, J. *J. Mol. Struct.* **1989**, *195*, 283.
(40) Librovich, N. B.; Maiorov, V. D. *Dokl. Akad. Nauk SSSR* **1975**, *225*, 1358.
(41) Librovich, N. B.; Sakun, V. P.; Sokolov, N. D. *Chem. Phys.* **1979**, *39*, 351.
(42) Librovich, N. B.; Sakun, V. P.; Sokolov, N. D. *Chem. Phys.* **1981**, *60*, 425.
(43) Kraemer, W. P.; Diekersen, G. H. F. *Chem. Phys. Lett.* **1970**, *5*, 463.
(44) Hayd, A.; Weidemann, E. G.; Zundel, G. *J. Chem. Phys.* **1979**, *70*, 86.
(45) Yeh, L. I.; Okumura, M.; Myers, J. D.; Price, J. M.; Lee, Y. T. *J. Chem. Phys.* **1989**, *91*, 7319.
(46) Okumura, M.; Yeh, L. I.; Myers, J. D.; Lee, Y. T. *J. Phys. Chem.* **1990**, *94*, 3416.
(47) Zygmunt, S. A.; Curtiss, L. A.; Iton, L. E. *J. Phys. Chem. B* **2001**, *105*, 3034.
(48) Termath, V.; Sauer, J. *Mol. Phys.* **1997**, *91*, 963.
(49) Wei, D.; Salahub, D. R. *J. Chem. Phys.* **1997**, *106*, 6086.
(50) Cheng, H.-P.; Krause, J. L. *J. Chem. Phys.* **1997**, *107*, 8461.
(51) Sagnella, D. E.; Tuckerman, M. E. *J. Chem. Phys.* **1998**, *108*, 2073.
(52) Chaban, G. M.; Jung, J. O.; Gerber, R. B. *J. Phys. Chem. A* **2000**, *104*, 2772.
(53) Yeh, L. I.; Lee, Y. T.; Hougen, J. T. *J. Mol. Spectrosc.* **1994**, *164*, 473.
(54) Suhm, M. A.; Watts, R. O. *Phys. Rep.* **1991**, *204*, 293.
(55) Anderson, J. B. *J. Chem. Phys.* **1976**, *65*, 4121.
(56) Anderson, J. B. *J. Chem. Phys.* **1975**, *63*, 1499.
(57) Bowman, J. M. *Acc. Chem. Res.* **1986**, *19*, 202.
(58) Chaban, G. M.; Jung, J. O.; Gerber, R. B. *J. Chem. Phys.* **1999**, *111*, 1823.
(59) Carter, S.; Bowman, J. M. *J. Phys. Chem. A* **2000**, *104*, 2355.
(60) Carter, S.; Bowman, J. M. *J. Chem. Phys.* **1998**, *108*, 4397.
(61) Carter, S.; Bowman, J. M.; Handy, N. C. *Theor. Chim. Acc.* **1998**, *100*, 191.
(62) Carter, S.; Culik, S. J.; Bowman, J. M. *J. Chem. Phys.* **1997**, *107*, 10458.
(63) MULTIMODE online documents and a more extensive list of references can be found at http://www.emory.edu/CHEMISTRY/faculty/bowman/multimode.
(64) Ojamäe, L.; Shavitt, I.; Singer, S. J. *J. Chem. Phys.* **1998**, *109*, 5547.
(65) Singer, S. J.; McDonald, S.; Ojamae, L. *J. Chem. Phys.* **2000**, *112*, 710.
(66) Moller, C.; Plesset, M. S. *Phys. Rev.* **1934**, *46*, 618.
(67) Frish, M. J.; Trucks, G. W.; Schlegel, H. B.; Gill, P. M. W.; Johnson, B. G.; Wong, M. W.; Foresman, J. B.; Robb, M. A.; Head-Gordon, M.; Replogle, E. S.; Gomperts, R.; Andres, J. L.; Raghavachari, K.; Binkley, J. S.; Gonzalez, C.; Martin, R. L.; Fox, D. J.; Defrees, D. J.; Baker, J.; Stewart, J. J. P.; Pople, J. A. Gaussian-92, Gaussian 92/DFT, Revision G.3. Revision G.3 ed.; Gaussian, Inc.: Pittsburgh, PA, 1993.
(68) Dunning, T. H., Jr. *J. Chem. Phys.* **1971**, *55*, 716.
(69) Kendall, R. A.; Dunning, T. H., Jr.; Harrison, R. J. *J. Chem. Phys.* **1992**, *96*, 6796.
(70) Kalos, M. H.; Levesque, D.; Verlet, L. *Phys. Rev.* **1974**, *9*, 2178.
(71) Reynolds, P. J.; Ceperley, D. M.; Alder, B. J.; Lester, W. A., Jr. *J. Chem. Phys.* **1982**, *77*, 5593.
(72) Hammond, B. L.; W. A. Lester, J.; Reynolds, P. J. *Monte Carlo Methods in Ab Initio Quantum Chemistry*; World Scientific: River Edge, NJ, 1994; Vol. 1.
(73) Bernu, B.; Ceperley, D. M.; W. A. Lester, J. *J. Chem. Phys.* **1990**, *93*, 552.
(74) Bernu, B.; Ceperley, D. M.; W. A. Lester, J. *J. Chem. Phys.* **1991**, *95*, 7782.
(75) Mathematica; Version 4 ed.; Wolfram Research, Inc.: Champaign, IL, 1999.
(76) Jastrow, R. *Phys. Rev.* **1955**, *98*, 1479.
(77) Kirkpatrick, S.; Gelatt, J. C. D.; Vecchi, M. P. *Science* **1983**, *220*, 671.
(78) Flyvbjerg, H.; Peterson, H. G. *J. Chem. Phys.* **1989**, *91*, 461.
(79) Barnett, R. N.; Reynolds, P. J.; Lester, W. A., Jr. *J. Comput. Phys.* **1991**, *96*, 258.
(80) Cheng, H.-P.; Barnett, R. N.; Landman, U. *Chem. Phys. Lett.* **1995**, *237*, 161.
(81) Tuckerman, M. E.; Marx, D.; Klein, M. L.; Parrinello, M. *Science* **1997**, *275*, 817.
(82) Watson, J. K. G. *Mol. Phys.* **1968**, *15*, 479.
(83) Watson, J. K. G. *Mol. Phys.* **1970**, *19*, 465.
(84) Bowman, J. M.; Huang, X.; Carter, S. *Spectrochim. Acta, Part A* **2002**, *58*, 825.
(85) Huang, X.; Carter, S.; Bowman, J. M. *J. Phys. Chem. B* **2002**, *106*, 8182.
(86) Leonard, C.; Handy, N. C.; Carter, S.; Bowman, J. M. *Spectrochim. Acta, Part A* **2002**, *58*, 825.
(87) Huang, X.; Carter, S.; Bowman, J. M. *J. Chem. Phys.* **2003**, *118*, 5431.
(88) (a) Tew, D. P.; Handy, N. C.; Carter, S. *Mol. Phys.* **2001**, *99*, 393. (b) Tew, D. P.; Handy, N. C.; Carter, S. *Phys. Chem. Chem. Phys.* **2001**, *3*, 1958.